Toward an optimized design of the LNG production process: Measurement and modeling of the solubility limits of p-xylene in methane and methane + ethane mixtures at low temperature

Paolo Stringari, Marco Campestrini, Nevin Gerek Ince, David Bluck, Seiya Hirohama, Freddy Garcia, Jean-Jacques Bartuel

Version of Record: https://www.sciencedirect.com/science/article/pii/S0378381222000310
Manuscript_908e8730841a6848e166432cf8d070b3

Toward an optimized design of the LNG production process:

Measurement and modeling of the solubility limits of p-xylene in methane and methane + ethane mixtures at low temperature

Paolo Stringari [1], Marco Campestrini [1], Nevin Gerek Ince [2], David Bluck [2], Seiya Hirohama [2], Freddy Garcia [3], Jean-Jacques Bartuel [4]

[1] MINES ParisTech, PSL University, CTP - Centre of Thermodynamics of Processes, 35 rue St Honoré 77300 Fontainebleau, France
[2] AVEVA, 26561 Rancho Pkwy S, Lake Forest, CA & Houston, TX, United States
[3] Total Energies, 2, place Jean Millier 92078 Paris La Défense CEDEX France
[4] Technip Energies, 6-8 Allée de l'Arche 92973 Paris La Défense Cedex France

Corresponding author e-mail: paolo.stringari@mines-paristech.fr

Abstract

Accurate knowledge of the solubility limits of impurities in LNG allows an optimized design of the purification units installed upstream of the liquefaction train and the prevention of solid formation in the main cryogenic heat exchanger that would reduce the performance of the heat exchanger, increase maintenance operations and cause potential safety problems. The solubility of p-xylene in methane and in methane + ethane (5 and 10% mole fraction of ethane) has been measured at p = 5 MPa from T = 183 down to T = 123 K. The experimental results have been obtained by a static-analytic method with analysis of the fluid phase samples by gas chromatography. Solubility of p-xylene in methane and methane + ethane mixtures has been measured for the first time in this temperature range. The obtained data have been modelled by the Soave-Redlich-Kwong (SRK) cubic Equations of State (EoS), tuning pure component parameters, alpha functions, and binary interaction parameters, considering thermodynamic constraints. A robust multi-phase flash algorithm was established for vapor-liquid-liquid-solid (VLLSE) equilibrium by applying phase stability analysis. The revamped thermodynamic methods and data allow accurate prediction of the multiple phase boundaries that can be present when cooling a typical natural gas mixture.

1 Introduction

Natural gas is predominantly methane, but contains significant quantities of ethane, propane, butanes and heavier hydrocarbons. Varying amounts of non-hydrocarbon impurities such as nitrogen,

the acidic components carbon dioxide and hydrogen sulfide, as well as water and mercury, are also naturally present. As the world works together towards reaching the Paris agreement objective of limiting global warming to well below 2 °C, switching from coal and other fossil fuels to methane is an attractive alternative in the generation of electricity or as a transportation fuel, because it produces less greenhouse gases - primarily carbon dioxide - for the same amount of energy produced. Additionally, methane is considered as a key player in the energy transition, as gas power plants are a perfect complement to renewable energies since, contrary to other electricity sources, they can rapidly compensate for the inherent instabilities of electricity from renewable sources such as solar and wind power.

Unfortunately, natural gas occurs and is often produced a considerable distance away from where it could be useful as a fuel. After a given distance, gas pipelines may be economically unattractive or even technically infeasible. For long distances, the best solution is to transport the natural gas in liquefied state (LNG), where it occupies approximately 600 times less volume than natural gas in its gaseous state, but containing the same amount of energy. This requires cooling of the natural gas to a temperature of around 110 K. At these temperatures, natural gas will be in liquid state at atmospheric pressure, meaning that the liquefied natural gas can be stored and transported without the need for tanks and vessels that have to withstand high pressures (at T = 110 K the vapor pressure of methane is close to the atmospheric pressure).

Before liquefaction, a certain level of purification is required. Typically, the acidic components, such as carbon dioxide and hydrogen sulfide, along with water and mercury, must be removed. Failure to remove them can cause corrosion in steel pipes and the amalgamation of mercury to aluminum in cryogenic heat exchangers. In addition, it will be necessary to remove most of the heavier hydrocarbons – mainly C5 and heavier – to reduce the risk that these components would crystallize at the cryogenic temperatures, causing fouling and potential damage to the refrigeration heat exchangers.

Accurate knowledge of the solubility limits of impurities in LNG allows an optimized design of the purification units installed upstream of the liquefaction train, which means lower installation costs, better energy efficiency of the overall process, and the prevention of solid formation in the main cryogenic heat exchanger. The specifications that must be achieved by the purification units for the different natural gas components in order to avoid crystallization risk are given by the manufacturers of cryogenic heat exchangers. A severe specification targets the group of aromatic components, including benzene, toluene, ethylbenzene and xylenes, named BTEX: as a rule of thumb, the total amount of BTEX in the feed of the main cryogenic heat exchanger must be < 1 ppm. This empirical specification has strong impact on the energy consumption of the purification units and in

turn on the margin in LNG sales. The knowledge of the solubility limits of BTEX in methane or natural gas-like mixtures is incomplete. The solubility of benzene in methane has been studied for temperatures from T = 90 to T = 278 K in [1-10]. The solubility of toluene in methane has been studied from T = 92 to T = 193 K in [2, 11]. In [12], solubility data for p-xylene in methane from T = 278 to T = 285 K and in ethane from T = 201 to T = 240 K, have been published. No data exist for the solubility of p-xylene in methane at temperatures representative of the operative conditions of the main cryogenic heat exchanger. In addition, no solubility data for o-xylene, m-xylene, and ethylbenzene in methane have been published in the scientific literature, to the authors' knowledge.

This work is the result of a research collaboration among academia and industry that includes a natural gas producer, an EPC (Engineering, Procurement, and Construction) company, and a simulation software company aiming at improving the knowledge of the solubility limits of some key impurities in LNG. Natural gas producers require an accurate design in process simulators to operate the liquefaction processes with confidence that crystallization will not occur, which would result in equipment fouling and downtime, potential asset integrity and safety problems. EPC companies, involved in the design and construction of LNG plants, need to be able to guarantee that the process which will be designed using simulation software will not have such operational issues. Process simulation developers have an interest in supplying the best combination of thermodynamic methods and data to its clients. Given the complexities of measuring low temperature phase equilibria including molecular solids, at the limits of solubility observed of impurities in natural gas, the expertise of specialized research groups is necessary to solve this industrial problem.

With the overall goal of creating comprehensive pure component thermo-physical property and thermodynamic model parameter data banks, combined with phase equilibrium calculations in the simulator that can handle multiple fluid and pure component solid phases, the authors have worked together to identify missing information, such as the solubility of BTEX at low temperatures, to measure that solubility, and to turn it into thermodynamic model parameters that can be used in the commercial process simulators typically used on the design and operation of LNG facilities. In this work, the solubility limits of p-xylene in methane have been measured at 5 MPa from T = 183 K down to T = 123 K. Among the xylenes, p-xylene is the one with the highest triple point temperature, as it can be seen from Table 1. Despite there are no literature data for the solubility limits of o-xylene and m-xylene in methane, the p-xylene triple point temperature allows the inference that it could present the highest risk of solidification among the xylenes. Moreover, in order to determine the effect of a richer natural gas on the solubility of p-xylene, solubility limits were also measured in methane + ethane mixtures with mole fractions of 5 and 10 % ethane at the same pressure and in the same temperature range as the measurements carried out for the p-xylene + methane system.

Table 1. Triple point properties for BTEX from the Design Institute for Physical Properties (DIPPR) 801 Database as reported in [12].

Component	CAS number	Chemical formula	T_t [K]	P_t [Pa]
Benzene	71-43-2	C6H6	278.68	4764
Toluene	108-88-3	C7H8	178.18	0.048
p-Xylene	106-42-3	C8H10	286.41	575.5
o-Xylene	95-47-6	C8H10	247.98	21.84
m-Xylene	108-38-3	C8H10	225.3	3.180
Ethylbenzene	100-41-4	C8H10	178.2	0.004

2 Experimental section

2.1 Apparatus

Solubility of solid p-xylene in liquid methane and methane + ethane mixtures were measured using a "static-analytic" method. The scheme of the apparatus is presented in Figure 1.

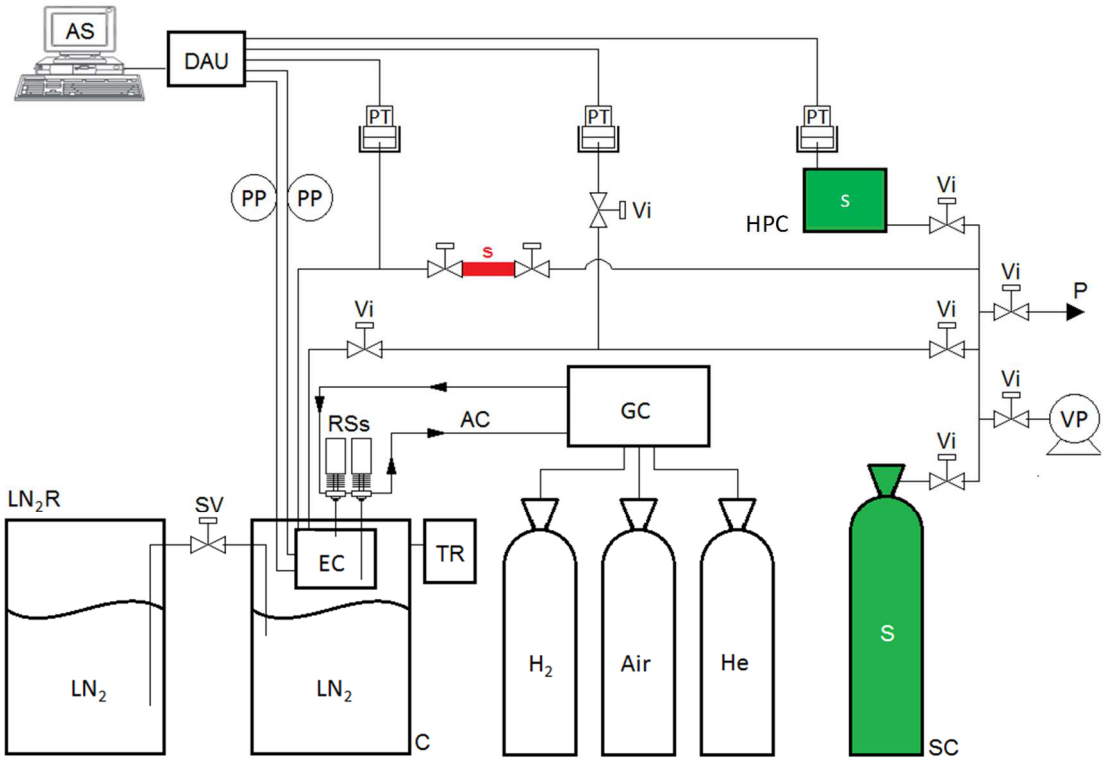

Figure 1. Scheme of the apparatus.
AC: analysis circuit; **Air**: air cylinder; **AS**: acquisition system; **C**: cryostat; **DAU**: data acquisition unit; **EC**: equilibrium cell; **GC**: gas chromatograph; **H_2**: H_2 cylinder; **He**: helium cylinder; **LN_2**: liquid nitrogen; **LN_2R**: liquid nitrogen ranger; **P**: purge; **PP**: platinum resistance thermometer probe; **PT**: pressure transducer; **RSs**: ROLSI® samplers; **S**: solvent; **s**: solute; **SC**: solvent cylinder; **SV**: solenoid valve; **TR** : temperature regulator; **Vi**: valve i; **VP**: vacuum pump.

About half of the Cryostat (C) in Fig. 1 was filled with Liquid Nitrogen (LN_2) from a Liquid Nitrogen Ranger (LN_2R) by means of a Solenoid Valve (SV). The Equilibrium Cell (EC) was then immersed in the N_2 vapor moving upwards in the cryostat and originating from the underlying LN_2 bath.

The equilibrium cell was loaded firstly with a small amount (about 1 mL) of p-xylene (solute, s), previously filled in a small tube between two valves, and then with the solvent (S) contained in a high pressure cell (HPC), previously filled from a solvent (methane or methane + ethane) cylinder (SC), at the temperature imposed by the Temperature Regulator (TR).

The analysis circuit (AC) was constituted of two electromagnetic ROLSI® Samplers (RSs) (allowing sampling the fluid phase from the top and the bottom of the equilibrium cell), the transfer line, and the Gas Chromatograph (GC). The samples were vaporized in the ROLSI® Samplers and mixed with the carrier gas (helium) flowing in the transfer line to the separation column located within the Gas Chromatograph.

In the equilibrium cell, temperature was measured by means of two calibrated Pt-100 probes (PP) and pressure by means of a calibrated Pressure Transducer (PT), connected to a Data Acquisition Unit (DAU). The temperature, pressure, and the signal obtained from the GC detectors were recorded in the Acquisition System (AS). A Purge (P) and a Vacuum Pump (VP) were installed for emptying the equilibrium cell and removing all mixture traces from the equipment, respectively.

The equilibrium cell assembly is shown in Figure. 2.

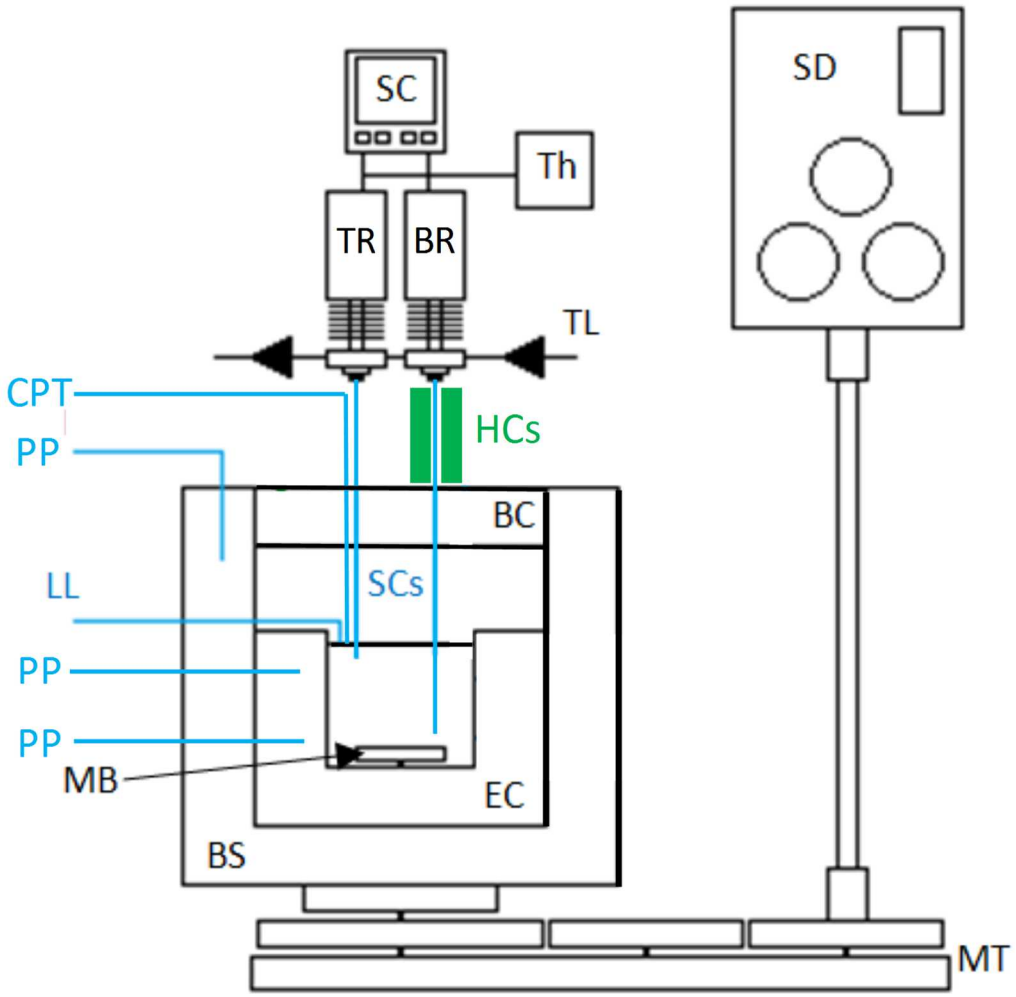

Figure 2. Details of the equilibrium cell assembly

BC: brass cap; **BS**: brass shell; **CPT**: connection to the pressure transducer; **EC**: equilibrium cell; **HCs**: heating cartridges; **LL**: loading line; **BR**: Bottom ROLSI® sampler; **MB**: magnetic bar; **MT**: mechanic transmission; **PP**: platinum resistance thermometer probe; **SC**: samplers control; **SCs**: sampling capillaries; **SD**: stirring device; **Th**: thermocouple; **TL**: transfer line; **TR**: Top ROLSI® sampler.

A variable-speed motor was used to drive a Magnetic Bar (MB) for stirring the content of the equilibrium cell and enhancing the mass and heat transfer for a faster achievement of phase equilibrium. Two Pt-100 probes, located at the bottom and at the top of the cell, allowed the detection of the vertical temperature gradient, that was between 0.2 and 0.5 K, depending on the level of liquid nitrogen in the cryostat and the measurement temperature.

An additional Pt-100 probe was used to measure the temperature in the Brass Shell (BS) and governs a heating resistance wrapping the external surface of the shell. The cold transferred by the N_2 vapor atmosphere was balanced by the regulation of the heat transferred to the equilibrium cell from the resistance, allowing achieving the temperature of the measurement and maintain it within ±0.05 K with respect to the target value.

The solvent could be loaded though the Loading Line (LL) or through the line connecting the cell and the pressure transducer (CPT), where the small tube containing the solute is also situated. Two stainless steel Sampling Capillaries (SCs) were connected to the bottom ROLSI® Sampler (BR) and the top ROLSI® Sampler (TR).

Finally, two Heating Cartridges (HCs) were installed and shown in Fig. 2, the former allowed regulating the temperature of the Brass Cap (BC); the latter enveloped the capillary of the BR and allowed maintaining the temperature of the capillary slightly higher than the temperature in the equilibrium cell for preventing solid formation in the capillaries (the capillary of the TR was heated by conduction from the HC of the capillary of the BR through an aluminum bridge).

2.2 Procedure

As first, vacuum was made in the equilibrium cell and the loading lines at ambient temperature for several hours. Then, the cell was inserted into the cryostat.

Known amounts of solute and solvent were introduced into the cell in order to obtain a mixture in the homogeneous gas phase. The amount of solute loaded into the cell has been determined measuring the mass difference of the small tube between the two valves (see section 2.1) when filled with the solute and when empty, and assuming that all the content of the small tube was pushed into the equilibrium cell when the solvent was loaded at high pressure passing through the small tube. The amount of solvent loaded into the equilibrium cell was determined by the pressure difference (at constant temperature) in the HPC before and after the loading, and knowing the density of the solvent through an equation of state. Adequate stirring (about 300 rpm) of the cell content was maintained during this procedure.

The global composition of the loaded mixture was determined by GC analysis of samples withdrawn by both the bottom and top ROLSI® Samplers and transferred to the GC to verify that the

solute was in excess with respect to its expected solubility limits at the temperature of the measurements. Solid formation was verified for each experimental point by comparison of the measured solubility of p-xylene and the mole fraction of p-xylene in the global composition.

Temperature was set to the first value of measurement. Once the temperature of the cell was stabilized, a known amount of solvent was loaded in the cell to reach the target pressure seeing that the system had underwent an isochoric cooling during the temperature decrease. This known amount of solvent has been used for calculating the new global composition of the mixture within the equilibrium cell, that has been successively compared with samples compositions.

Phase equilibrium has been assumed to be achieved when the pressure and the two temperature readings were stabilized to within their instrument uncertainty, for at least 10 minutes. The time for achieving temperature and pressure stability ranged between 6 and 12 hours depending on the temperature difference with respect to the previous measurement and the necessity to load new liquid nitrogen in the cryostat (that perturbs temperature stability). After stabilization of temperature and pressure, the sampling procedure began and was continued until a minimum of 12 samples of repeatable composition (after GC analysis) were obtained from top and the bottom samplers. The average composition of these samples corresponds to the composition of one experimental point. The temperature was successively decreased and further solvent was loaded in the equilibrium cell for increasing the pressure up to the target value.

2.3 Chemicals

Suppliers and purities for the chemicals used in this work are presented in Table 2. The second column of the Table reports the purity for pure components or the composition for mixtures. For the methane + ethane mixtures with mole fractions of 5 and 10 % ethane, the composition reported in the second column of the table is the one certified by the supplier (uncertainty is 0,020 mol/mol %); no further analysis has been carried out.

Table 2. Purities and suppliers of the chemicals used in this work.

Chemical	Purity or composition (mol/mol %)	Supplier
Methane	99.995	Messer
Methane + Ethane (5 %)	95.036 (Methane)	Air Liquide
Methane + Ethane (10 %)	89.955 (Methane)	Air Liquide
p-Xylene	99	Merck

2.4 Analysis

Samples compositions have been analyzed using a gas chromatograph (Perichrom PR 2100). The separation of methane and p-xylene has been obtained through a column of type 15% APIEZON-L, 80/100 mesh, 1/8 inch external diameter, 2 mm internal diameter, 1.8 m long. The temperature of the oven has been set at 453 K and the pressure of the carrier gas (helium) at 220 kPa. For each sample, the number of moles of solvent has been determined using the Thermal Conductivity Detector (TCD), while the one of the solute by the Flame Ionization Detector (FID). The response of the TCD and the FID has been calibrated by the analysis of known amount of each component. Known volumes of methane and methane + ethane mixtures, which are gas at ambient temperature and atmospheric pressure, have been fed to the TCD using a graduated calibration syringe. The volumes have been converted in number of moles using the equation of state of methane and ethane at the measured ambient temperature and at the atmospheric pressure. In order to calibrate the FID detector with small quantities of p-xylene, as the ones expected in the samples at low temperature, where p-xylene solubility is very low, p-xylene has been diluted in a liquid solvent in a vial. The composition of the solution was determined by weighing the vial with a precision balance at each different step of the preparation of the solution. Known volumes of solution have been fed to the FID through a graduated calibration syringe. The volumes of solution (assumed as ideal solution) have been related to the number of moles of p-xylene by knowing the density of the two components and the composition of the liquid mixture. The TCD and FID responses have been related to the different amount of moles of each component by a polynomial. The correlation error of each polynomial has been included in the calculation of the uncertainty of the measured p-xylene solubility.

ROLSI® Samplers are connected to the gas chromatograph through a transfer line. The transfer line is heated at a temperature 10 K higher than the solute normal boiling temperature to avoid its potential condensation.

3 Experimental results

The experimental results for the limits of solubility of p-xylene in methane and methane+ethane mixtures between T = 123 and T = 183 K are presented in Table 3.

Table 3. Experimental results obtained for the solubility of p-xylene in methane and methane + ethane mixtures.

T: experimental temperature; P: experimental pressure; z_{pC8H10} : global composition of p-xylene; x_{pC8H10} : mole fraction of p-xylene in the liquid solvent; U : expanded (k=2) uncertainty. N° points: number of experimental points measured for each experimental temperature. N° samples: total number of samples corresponding to all experimental points for each experimental temperature.

T [K]	P [MPa]	z_{pC8H10} [ppm]	x_{pC8H10} [ppm]	U(T) [K]	U(P) [kPa]	U(x_{pC8H10}) [ppm]	N° points	N° Samples
Solvent Methane								
183.10	4.897	111-216	20.1	0.03	1	0.3	9	58
180.63	4.959	130-251	24.1	0.06	3	0.5	3	45
178.09	5.044	126-246	25.8	0.05	3	0.5	3	39
175.31	5.139	119-231	24.3	0.06	3	0.6	3	51
172.83	5.099	98-191	20.8	0.04	2	0.4	4	22
167.75	4.930	103-207	18.0	0.06	3	0.5	3	37
162.45	5.479	91-177	12.9	0.03	2	0.2	7	76
158.51	5.344	97-189	11.3	0.08	4	0.5	2	29
153.70	4.988	87-168	8.3	0.03	2	0.3	7	38
148.71	5.417	91-170	7.3	0.08	7	0.4	2	26
143.69	5.535	82-159	4.8	0.05	5	0.3	3	27
138.24	5.410	73-159	3.9	0.06	5	0.2	3	31
133.28	5.613	79-296	2.8	0.03	3	0.2	6	37
123.52	5.099	76-145	1.4	0.03	3	0.1	9	58
Solvent: Methane + Ethane (x_{CH4}/x_{C2H6}=95/5 molar)								
183.06	5.085	1020	63.9	0.06	3	1.4	2	25
173.07	5.232	941	47.0	0.06	5	0.9	2	32
162.52	5.134	884	26.5	0.08	6	0.6	1	13
153.90	5.048	850	13.0	0.08	5	0.4	1	18
143.48	5.212	812	5.2	0.06	5	0.3	2	14
133.68	4.807	785	2.0	0.08	9	0.1	1	19
123.47	5.513	757	0.7	0.08	1	0.1	1	18
Solvent: Methane + Ethane (x_{CH4}/x_{C2H6}=90/10 molar)								
182.95	5.259	631	92.5	0.05	2	1.8	3	28
172.76	4.910	585	65.3	0.08	4	2.0	1	15
162.44	5.478	550	38.5	0.04	4	1.8	4	35
153.72	5.214	533	17.5	0.06	3	0.8	2	15
143.59	4.880	512	7.6	0.08	6	0.4	1	10
133.23	4.835	493	3.1	0.08	11	0.3	1	10
123.54	4.918	432	1.0	0.06	5	0.1	2	15

Experimental conditions of temperature and pressure are given respectively in the first and second column of Table 3. The global composition of p-xylene in the equilibrium cell and its composition in the liquid solvent at the solid-liquid equilibrium are indicated in the 3rd and 4th column, respectively.

For the binary mixture CH_4+pC_8H_{10}, a range of global composition is indicated in the 3rd column seeing that 3 experimental campaigns have been carried out (each with a different global composition).

The mole fractions have been obtained from the composition analysis carried out by gas chromatography (GC analysis). The expanded (k=2) uncertainties related to temperature, pressure, and mole fraction are reported in the 5th, 6th, and 7th column, respectively. The last columns of Table 3 give the number of experimental points that have been measured for the generic experimental temperature and the total number of samples considering all the experimental points; the values in Table 3 are then averaged values in case of N° points > 1.

Results within Tab. 3 are shown in Figures 3 and 4. Figure 3 shows the variation of the solubility of p-xylene as a function of temperature, whereas Fig. 4 is a plot of the logarithm of the same experimental values as a function of the reciprocal temperature.

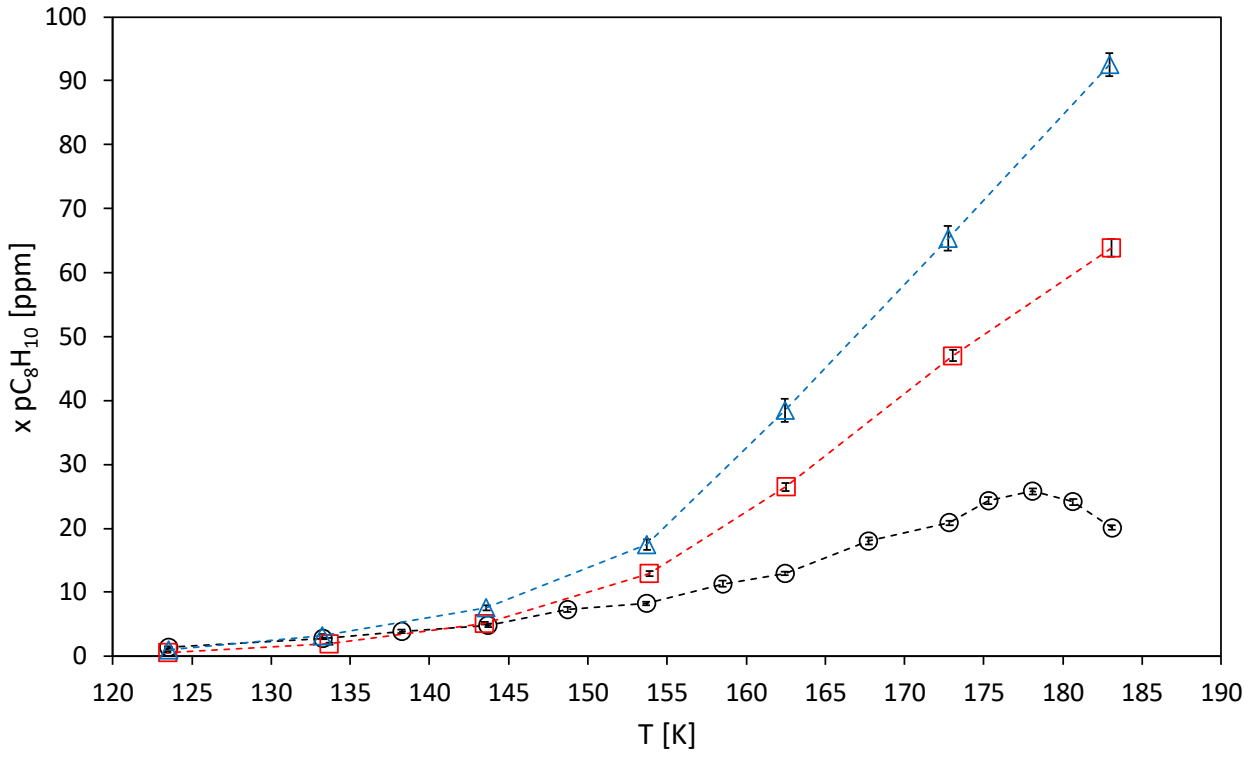

Figure 3. Solubility of pC_8H_{10} in CH_4 and CH_4+C_2H_6 mixtures with respect to temperature. ○ : solubility of p-xylene in liquid methane; □ : solubility of p-xylene in liquid 95% methane + 5% ethane; Δ : solubility of p-xylene in liquid 90% methane + 10% ethane. Dotted lines are merely straight lines connecting the experimental points for each solvent for the reader convenience.

Three series of measurements have been carried out in order to obtain an accurate description of the solubility of p-xylene in liquid methane, in particular between T = 173 K and T = 183 K, where the solubility variation strongly depend on the variation of the density of the solvent. Furthermore, this allowed validating the experimental procedure used for the measurements.

Figures 3 and 4 allow pointing out that the solubility of p-xylene in methane does not decrease monotonically in the studied temperature range, but have a maximum at about 178 K. Moreover, the solubility curve of p-xylene in methane crosses the solubility curve of p-xylene in methane + ethane (5%) at about 143 K (1/T = 0.007 K^{-1}) and the one of p-xylene in methane + ethane (10%) at about 130 K (1/T = 0.0077 K^{-1}). In the authors' interpretation, the first behavior is influenced by the dependence of the p-xylene solubility on the solvent molar density, ρ. In particular, the maximum in the solubility curve of p-xylene in methane is caused by the density change with temperature in the vicinity of the critical point of methane. The fact that the solubility curve of p-xylene in methane crosses the solubility curves in methane + ethane deserves further experimental investigations to be confirmed. Nevertheless, from Figure 5 it can be noticed that at 5 MPa the molar density of methane varies more quickly with temperature than the molar density of the methane + ethane mixtures. As a consequence, the molar density of methane at the highest temperatures of this study is lower than the one of the methane + ethane mixtures, but this relation inverts at low temperature. This behavior could help explaining the crossing of the solubility curves, if this behavior will be confirmed by further experiments.

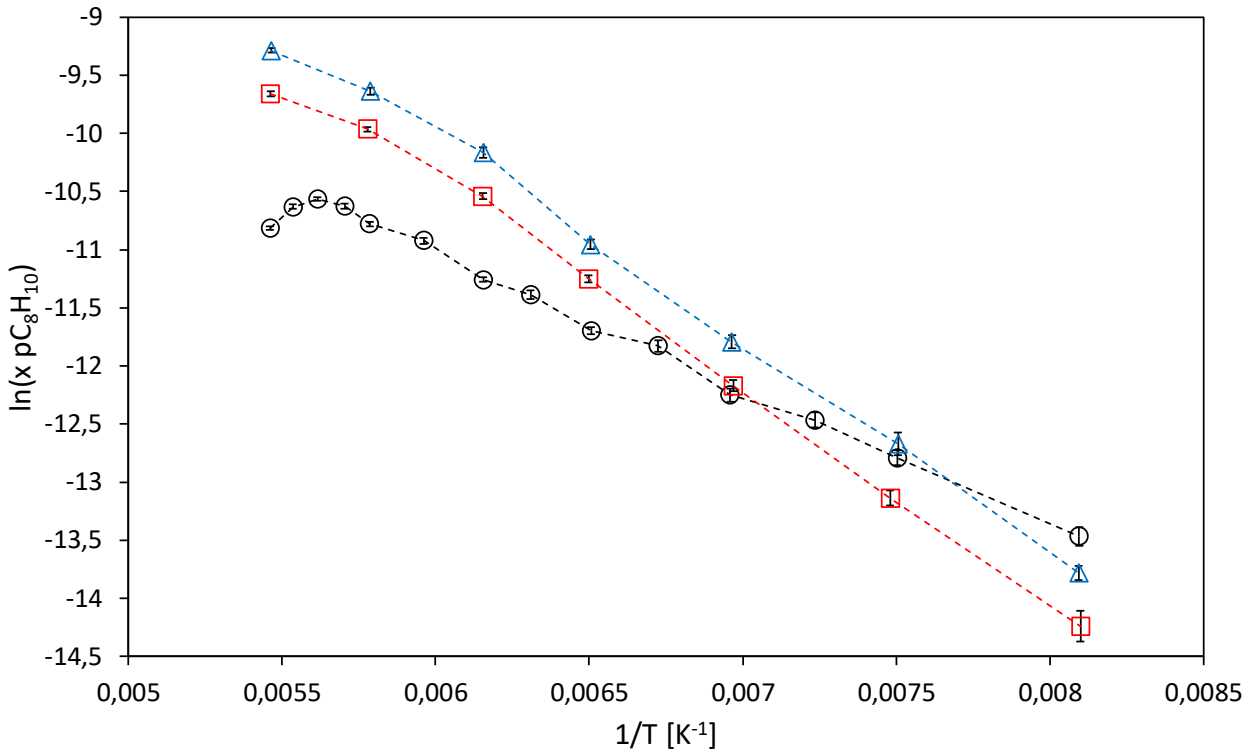

Figure 4. Logarithm of the solubility of pC_8H_{10} in CH_4 and CH_4+C_2H_6 mixtures with respect to reciprocal temperature.
○ : solubility of p-xylene in liquid methane; □ : solubility of p-xylene in liquid 95% methane + 5% ethane; Δ : solubility of p-xylene in liquid 90% methane + 10% ethane. Dotted lines are merely straight lines connecting the experimental points for each solvent for the reader convenience.

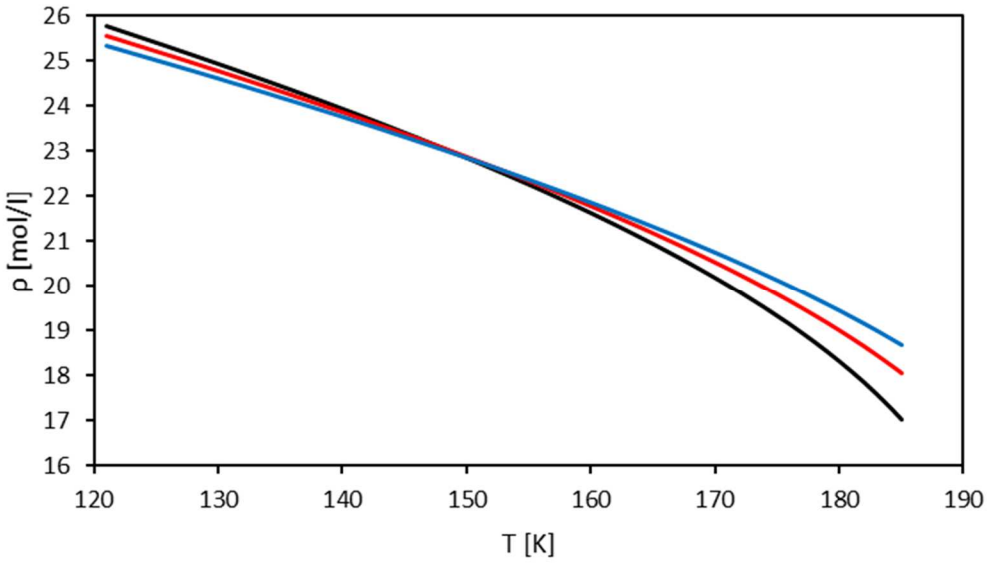

Figure 5. Molar density of CH_4 and CH_4+C_2H_6 mixtures at 5 MPa with respect to temperature. ─ : pure methane; ─ : 95% methane + 5% ethane; ─ : 90% methane + 10% ethane. The curves in the figure have been calculated using the reference equations implemented in the software REFPROP 8.0 [13].

4 Modeling and Discussion

The modeling approach is based on the fundamental assumption that hydrocarbons crystalize as pure components and may do so when the system temperature is below the liquid-solid phase boundary that is usually close to the pure component's triple point temperature at the system pressure.

4.1 Regression of pure component parameters

The pure component data such as critical temperature, pressure, ideal gas specific heat capacity, solid heat capacity, saturated vapor pressure and solid density for methane, ethane and p-xylene have been gathered from available sources such as the Design Institute for Physical Properties (DIPPR) 801 dataset [14] and NIST TDE [15]. Saturated vapor pressure data from NIST TDE have been extracted and all the data that were either outside feasible ranges (less than triple temperature or pressure or greater than critical temperature and pressure) were eliminated. For pure components, the parameters of the equation of state have been regressed from saturation pressure (liquid-vapor equilibrium) data.

The Soave-Redlich-Kwong Equation of State (EoS) [16], Eq. (1), has been selected as thermodynamic model in this study:

$$P = \frac{RT}{V-b} - \frac{a(T_r)}{V(V+b)} \tag{1}$$

where $a(T_r) = \alpha(T_r)a_c$. The values of a_c and b_c are obtained from pure-component critical properties, Eqs. (2) and (3):

$$a_c = \frac{0.42747\ (RT_c)^2}{P_c} \tag{2}$$

$$b_c = \frac{0.08664\ RT_c}{P_c} \tag{3}$$

Using the universal equation, Eq. (4), for the Soave-Redlich-Kwong Eos [17],

$$\frac{\alpha(T_r)}{T_r} = 1 + \sum_{i=1}^{N=13} C_i \left[ln\left(\frac{T_r}{P_r}\right)\right]^i \tag{4}$$

where $P_r = P(T)/P_c$ and $T_r = T/T_c$, a very accurate initial estimate of $\alpha(T_r)$ at each experimental (T_r, P_r) was obtained. By equating liquid and vapor fugacities at (T_r, P_r) corresponding to each experimental point reported in the literature, $\alpha(T_r)$ values have been iteratively adjusted. Then, $\alpha(T_r)$ was correlated to the Twu-Bluck-Cunningham-Coon (TBC) alpha formulation [18], Eq. (5):

$$\alpha(T_r) = {T_r}^{N(M-1)} exp\left[L\ (1 - {T_r}^{NM})\right] \tag{5}$$

Where L, M and N are refitted parameter reported in Table 4. In the refitting process, the coefficients, L, M, and N, were constrained to ensure that $\alpha(T_r)$ exactly reproduces the triple point and obey constraints given by Le Guennec et al. [19] to ensure realistic extrapolation of $\alpha(T_r)$ beyond T_c.

Table 4. Critical properties of the chemicals used in this work and re-fitted parameters for the TBC alpha formulation in the SRK EoS.

Component	T_c	P_c	Parameters of the $\alpha(T_r)$ function in SRK EoS		
	[K]	[MPa]	L	M	N
Methane	190.56	4.599947	0.427600	0.946600	1.119500
Ethane	305.41	4.879	0.39763	0.87477	1.33414
p-xylene	616.19	3.52610	0.770879	0.907107	1.228179

4.2 Regression of binary interaction parameters

The SRK EoS is extended to mixtures using the one-fluid approach where parameters *a* and *b* are obtained through mixing rules. With *i* and *j* denoting the components, *a* and *b* are obtained from equations (6) to (9):

$$b = \sum_i x_i b_i \tag{6}$$

$$b_i = b_{c,i} \tag{7}$$

$$a = \sum_i \sum_j x_i\, x_j \sqrt{a_i a_j}\left(1 - k_{ij}(T)\right) \tag{8}$$

$$a_i = \alpha_i\left(T_{r,i}\right) a_{c,i} \tag{9}$$

where x_i and x_j are the mole fractions of components *i* and *j*, and k_{ij} is the binary interaction parameter for components *i* and *j*.

For methane + ethane, methane + p-xylene, and ethane + p-xylene, VLE and SLE data have been extracted from NIST TDE including experimental measurements from Section 3. VLE (P, T, x, y) data at constant temperature from the literature have been initially used for regressing the binary interaction parameter values (k_{ij}) at discrete temperatures. The prediction of SLE using the obtained binary interaction parameters has been compared with the experimental values presented in Section 3. Because the experimentally measured solubilities were not well predicted using k_{ij} fitted to the VLE literature data, k_{ij} was exactly fitted to each solubility measurement (P, T, x), equating solid and liquid fugacities. The method for predicting the pure component solid fugacity, based on the fluid phase fugacity at the solid-liquid phase boundary, the heat of fusion, and solid phase enthalpy, can be found in the Supporting Information. For the methane + p-xylene mixture, k_{ij} values determined from the experimental solubility data obtained in this work have been correlated using a second order polynomial in temperature (k_{ij} = -0.344 + 4.64×10^{-3} T -1.36×10^{-5} T^2). In this fitting procedure,

accuracy of prediction needed to be compromised as temperature approached the critical temperature of methane (190.56 K, see Table 4) in order to maintain a simple functional form, as shown in Figure 6.

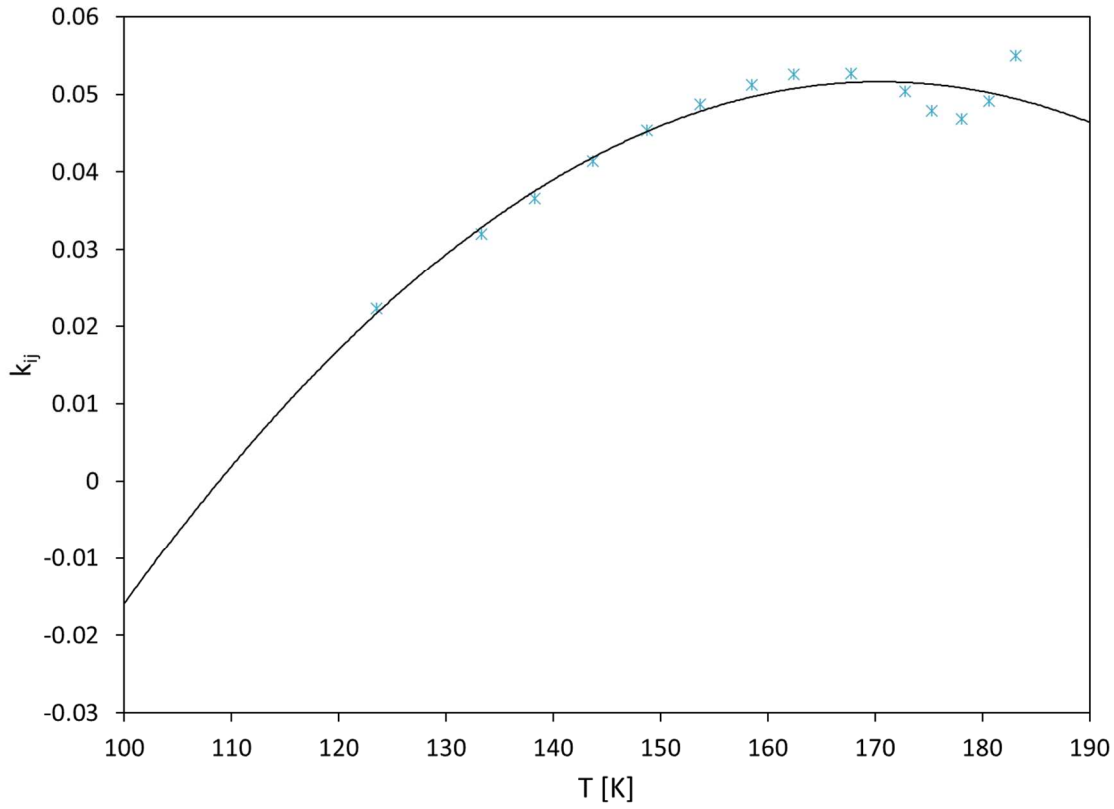

Figure 6. Binary interaction parameters (k_{ij}) as a function of temperature. Symbols are the values of k_{ij} for the SRK EoS obtained to represent exactly each experimental point. The continuous curve is a second order polynomial ($k_{ij} = -1.36\times10^{-5}\ T^2 + 0.00464\ T - 0.344$) regressed on the k_{ij} values.

4.3 Discussion

The p-xylene solubility in liquid methane calculated using the SRK EoS with the temperature-dependent k_{ij} has been compared with the experimental values of solubility, as shown in Figure 7. The comparison shows a good agreement between the calculated values and the experimental ones reported in Table 3. Table 5 provides the quantitative model performance compared to experimental data and shows the average absolute deviation (AAD%) value for each data point. The overall AAD% for the model is 6%. As expected, the region closer to the critical temperature of methane is under-predicted due to compromise in the binary interaction parameter fitting process.

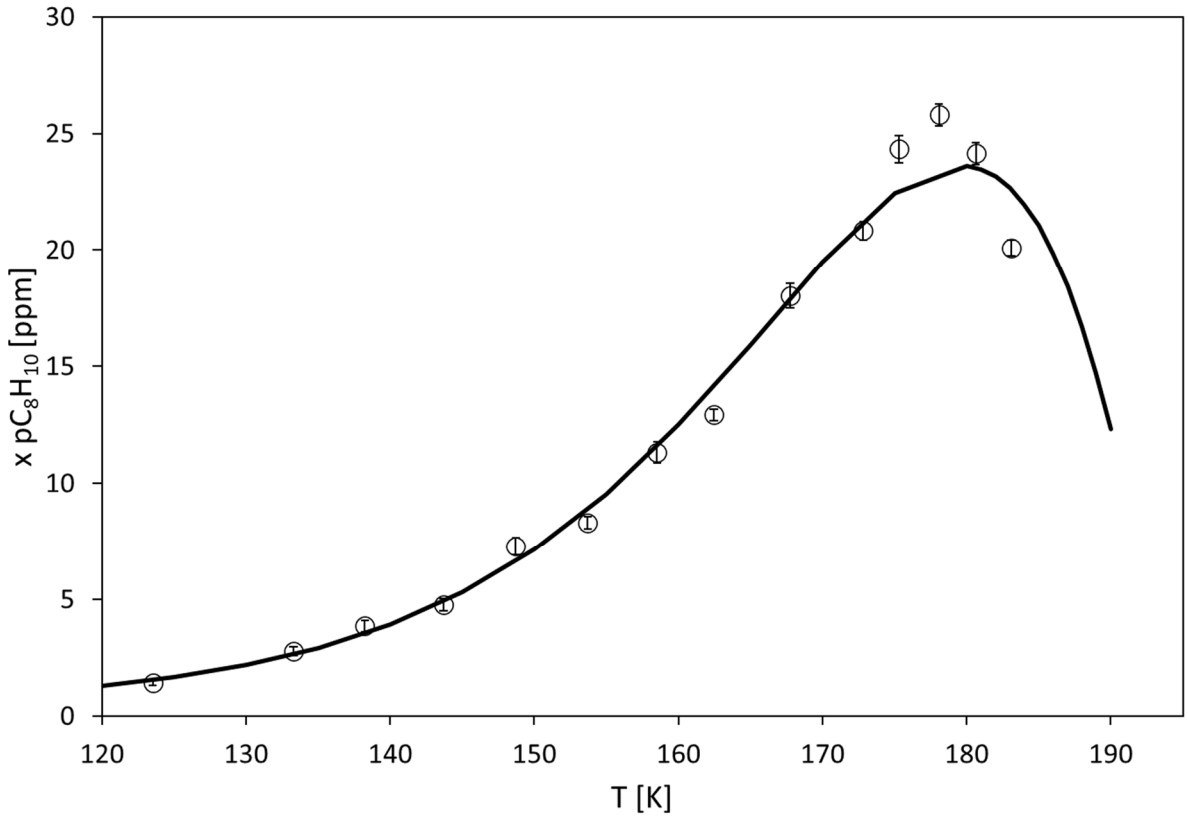

Figure 7. Comparison of the experimental solubility data (Table 3) of p-xylene in methane and the solubility values calculated using the SRK EoS with the second order polynomial expression of k_{ij} (Figure 6). ○ : experimental solubility of p-xylene in liquid methane; ─ : Solubility calculated using the SRK EoS.

The prediction of the solubility of p-xylene in methane and ethane mixtures has been also carried out. If a null value of the binary interaction parameter is used for the pC_8H_{10} + C_2H_6 mixture, the predicted solubility match well with experimental data in the case of 5% of ethane in the mixture, but overestimate the solubility in the case of 10% of ethane in the mixture. The optimal value of the binary interaction parameter between pC_8H_{10} and C_2H_6 has been found to be 0.04. Solid lines in Figure 8 display the comparison between the model and the data when k_{ij} for pC_8H_{10} + C_2H_6 is zero and dashed lines present results when k_{ij} for pC_8H_{10} + C_2H_6 is 0.04. As a conclusion, this shows a need for a binary interaction parameter for pC_8H_{10} + C_2H_6. For extending the validity range of the model, the recent data of Siahvashi et al. [12] for the solubility of pC_8H_{10} in both CH_4 and C_2H_6 should be included in the regression procedure.

Table 5. Comparison of experimental and modeling results for the solubility of p-xylene in methane and methane + ethane mixtures (k_{ij} for pC_8H_{10} - C_2H_6 equal to 0.04).

T [K]	P [bar]	x_{pC8H10} Experimental [ppm]	x_{pC8H10} Modeling [ppm]	AAD%
Solvent: Methane				
183.10	48.97	20.1	22.60	12
180.63	49.59	24.1	23.54	2
178.09	50.44	25.8	23.49	9
175.31	51.39	24.3	22.59	7
172.83	50.99	20.8	21.29	2
167.75	49.30	18.0	17.88	1
162.45	54.79	12.9	14.13	9
158.51	53.44	11.3	11.56	2
153.70	49.88	8.3	8.88	7
148.71	54.17	7.3	6.64	9
143.69	55.35	4.8	4.92	3
138.24	54.10	3.9	3.54	8
133.28	56.13	2.8	2.64	5
123.52	50.99	1.4	1.54	9
Solvent: Methane + Ethane (xCH_4/xC_2H_6=95/5 molar)				
183.06	50.85	63.9	53.66	16
173.07	52.32	47.0	39.79	15
162.52	51.34	26.5	2309	13
153.90	50.48	13.0	13.78	6
143.48	52.12	5.2	7.17	38
133.68	48.07	2.0	3.83	91
123.47	55.13	0.7	2.14	206
Solvent: Methane + Ethane (xCH_4/xC_2H_6=90/10 molar)				
182.95	52.59	92.5	99.75	8
172.76	49.10	65.3	60.94	7
162.44	54.78	38.5	34.85	9
153.72	52.14	17.5	19.72	13
143.59	48.80	7.6	9.97	31
133.23	48.35	3.1	5.05	63
123.54	49.18	1.0	2.81	181

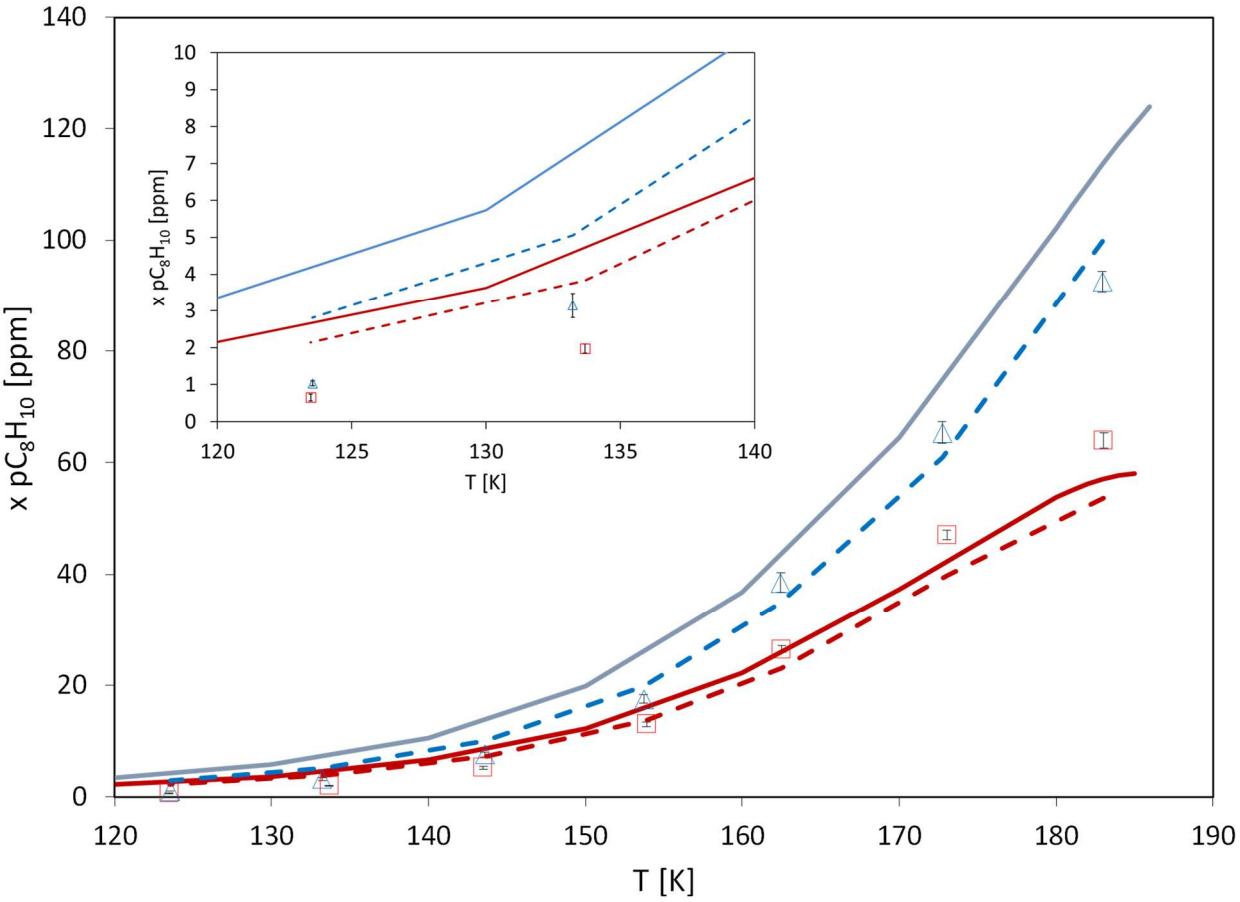

Figure 8. Comparison of experimental data (Table 3) and model results for pC_8H_{10} in CH_4+C_2H_6 mixtures

□ : experimental solubility of p-xylene in liquid 95% methane + 5% ethane; Δ : experimental solubility of p-xylene in liquid 90% methane + 10% ethane. Solid lines are obtained when k_{ij} for pC_8H_{10} + C_2H_6 is 0.0. Dotted lines are obtained when k_{ij} for pC_8H_{10} + C_2H_6 is 0.04. Red and blue lines are for the solvent containing 5% and 10% of ethane, respectively. Inset figure shows the comparison at the lower temperature range (120K-140K).

5 Conclusions

The solubility of p-xylene in methane and mixtures of methane and ethane have been measured for the first time at temperatures representative of the operative conditions of the main cryogenic heat exchanger. The experimental results show that, among the BTEX of known solubility, p-xylene is the least soluble in methane (1.4 ± 0.1 ppm at 123.52 K), and therefore it presents the highest risk of crystallization. At the pressure of the measurements (5 MPa), the solubility of-p-xylene in methane shows a strong dependence on the density change of methane with temperature close to its critical temperature. The addition of ethane increases the solubility of p-xylene at high temperature, but it has the opposite effect at low temperature. Authors recommend further studies in the low-temperature region to confirm this behavior. A potential explanation of the temperature-dependence of the influence of ethane on the solubility of p-xylene in methane could be found in the change of the density of the solvent (methane or methane + ethane) with temperature. The low solubility of p-xylene in natural gas is a key aspect for the design of purification units in the natural gas liquefaction process, in particular the scrub column. For such a purpose, parameters of the SRK EoS have been regressed in order to give an accurate representation of the solid-liquid equilibrium of p-xylene + methane and methane + ethane mixtures. The developed model is a suitable tool to be integrated in the process simulators used in the design of the liquefaction process.

References

[1] A. Neumann, R. Mann, Solubility of solid hydrocarbons and methanol in liquid methane, Kaltetechnik-Klimatisierung 22 (1970) 182–183.

[2] G.P. Kuebler, C. McKinley, Solubility of Solid Benzene, Toluene, n-Hexane, and n-Heptane in Liquid Methane, in: K.D. Timmerhaus (Ed.), Advances in Cryogenic Engineering, US, Springer, 1995, pp. 320–326.

[3] M. Teller, Experimental and theoretical investigation of solid-liquid phase equilibria of binary mixtures at low temperatures, TU Berlin (1982), 1–157.

[4] K.D. Luks, J.D. Hottovy, J.P. Kohn, Three-phase solid-liquid-vapor equilibria in the binary hydrocarbon systems methane-n-hexane and methane-benzene, J. Chem. Eng. Data 26 (1981) 402–403, doi: 10.1021/JE00026A016.

[5] M.P.W.M. Rijkers, M. Malais, C.J. Peters, J. de Swaan Arons, Experimental determination of the phase behavior of binary mixtures of methane + benzene: part I. Vapor + liquid, solid benzene + liquid, solid benzene + vapor and solid benzene + liquid + vapor equilibria, Fluid Phase Equilib. 77 (1992) 327–342, doi: 10.1016/0378-3812(92)85112-L.

[6] GPSA. Section 16 - Hydrocarbon Recovery. GPSA Engineering Databook, 13th ed. Tulsa, Oklahoma; 2012.

[7] A. Neumann, R. Mann, W.D. von Szalghary, The solubility of solid benzene in liquid hydrocarbons, Kaltetechnik-Klimatisierung 24 (1972) 145–149.

[8] T.J. Hughes, M.E. Kandil, B.F. Graham, K.N. Marsh, S.H. Huang, E.F. May, Phase equilibrium measurements of (methane+benzene) and (methane+methylbenzene) at temperatures from (188 to 348) K and pressures to 13MPa, J. Chem. Thermodyn. 85 (2015) 141–147, doi: 10.1016/j.jct.2014.12.031.

[9] A. Siahvashi , S.ZS. Al Ghafri , E. F. May, Solid-fluid equilibrium measurements of benzene in methane and implications for freeze-out at LNG conditions, Fluid Phase Equilib. 2020, 519, 112609, doi: https://doi.org/10.1016/j.fluid.2020.112609.

[10] A. Siahvashi, S.ZS. Al Ghafri, B.F. Graham, E.F. May, Experimental study of impurity freeze-out in ternary methane + ethane + benzene mixtures with applications to LNG production, J. Nat. Gas Sci. Eng. 90 (2021) 103918, doi.org/10.1016/j.jngse.2021.103918.

[11] F. Kurata, Solubility of heavier hydrocarbons in liquid methane, GPA RR-14, 1975.

[12] A. Siahvashi, S.ZS. Al Ghafri, T.J. Hughes, B.F. Graham, S.H. Huang, E.F. May, Solubility of p-xylene in methane and ethane and implications for freeze-out at LNG conditions, Exp. Therm. Fluid Sci. 105 (2019) 47–57, doi: 10.1016/j.expthermflusci.2019.03.010.

[13] E. Lemmon, M. Huber, M. McLinden, NIST Standard Reference Database 23: Reference Fluid Thermodynamic and Transport Properties-REFPROP, Version 8.0, National Institute of Standards and Technology, Standard Reference Data Program, Gaithersburg, 2007.

[14] W.V. Wilding, R.L. Rowley, J.L. Oscarson, DIPPR® Project 801 evaluated process design data, Fluid Phase Equilib., 150–151 (1998) 413–420.

[15] V. Diky, R.D. Chirico, M. Frenkel, A. Bazyleva, J.W. Magee, E. Paulechka, A. Kazakov, E.W. Lemmon, C.D. Muzny, A.Y. Smolyanitsky, S.A. Townsend, K. Kroenlein, ThermoData Engine (TDE) Version 10.1 - Pure Compounds, Binary Mixtures, Ternary Mixtures, and Chemical Reactions, NIST Standard Reference Database 103b. National Institute of Standards and Technology, Standard Reference Data Program; Gaithersburg, MD: 2016. http://nist.gov/srd/nist103b.cfm.

[16] G. Soave, Equilibrium Constants from a Modified Redlich-Kwong Equation of State. Chem. Eng. Sci., 27 (1972) 1197–1203, doi: 10.1016/0009-2509(72)80096-4.

[17] G. Soave, Direct calculation of pure-compound vapour pressures through cubic equations of state, Fluid Phase Equilib., 31 (1986) 203–207, doi: 10.1016/0378-3812(86)90013-0.

[18] C.H. Twu, D. Bluck, J.R. Cunningham, J.E. Coon, A Cubic Equation of State with a New Alpha Function and a New Mixing Rule, Fluid Phase Equilib. 69 (1991) 33–50, doi: 10.1016/0378-3812(91)90024-2.

[19] Y. Le Guennec, R. Privat, S. Lasala, J.N. Jaubert, On the imperative need to use a consistent α-function for the prediction of pure-compound supercritical properties with a cubic equation of state, Fluid Phase Equilib. 445 (2017) 45–53, doi: 10.1016/j.fluid.2017.04.015.